Publications of the Astronomical Society of the Pacific, 137:054402 (12pp), 2025 May https://doi.org/10.1088/1538-3873/add37a

Spectral Structure of the Solar Inertial Motion from 12999 BC to 16998 AD

Nicola Scafetta[1] and Franco Milani[2]
[1] Department of Earth Sciences, Environment and Georesources, University of Naples Federico II, Complesso Universitario di Monte S. Angelo, Naples, Italy; nicola.scafetta@unina.it
[2] Associazione Astronomica Euganea, via C. Battisti 59D, 35010 Limena (Padua), Italy
Received 2024 December 4; revised 2025 April 18; accepted 2025 May 2; published 2025 May 21

Abstract

The solar inertial motion (SIM) reflects the dynamics of the planetary system around the Sun. To study and accurately model the frequency domain of the SIM is of great importance as any function of the orbits as a whole is expected to be spectrally coherent with it. This study proposes a comprehensive spectral model for accurately reconstructing the SIM frequencies using the orbital periodicities of the Jovian planets. Specifically, we utilize high-precision records of the SIM (from 12999 BC to 16998 AD) obtained from the latest JPL ephemeris files DE440 and DE441 to estimate the temporal sequences of the periods and lengths of the SIM orbital cycles. The 30,000 yr-long SIM records are used to evaluate SIM periodograms with the highest spectral resolution currently available. The obtained sharp spectra enabled the validation of our spectral model constructed using the orbital near-commensurabilities of Jupiter, Saturn, Uranus, and Neptune. We provide a brief overview of the primary mathematical properties of the proposed model and, in particular, we demonstrate that it can be conveniently represented and managed through the adoption of a vectorial formulation, which allows for the rapid calculation of each SIM periodicity. This formulation employs the synodic periods of each planet pair as constructors, in addition to the orbital period of a single planet (e.g., Jupiter alone). Thus, we demonstrate that the proposed spectral model accurately identifies the specific planetary origin of each frequency of the SIM, which are numerous, and illustrate that they are clustered around specific frequency values. Finally, we also show that these SIM frequency clusters are well centered around periods given by the harmonic model $P_n \approx 179/(n-1)$ yr (where $n \geqslant 2$ is the cluster order) up to at least the 20th harmonic and discuss the significance of some of the long millennial SIM periodicities.

Supplementary material for this article is available online

Unified Astronomy Thesaurus concepts: Center of mass (216); Orbital resonances (1181); Astronomy data modeling (1859); Time series analysis (1916); Planetary alignment (1243); Solar-planetary interactions (1472); The Sun (1693); Ephemerides (464); Solar motion (1507)

1. Introduction

Solar inertial motion (SIM) describes the movement of the Sun around the Solar System Barycenter (SSB). This motion is primarily influenced by the gravitational attraction of the most massive planets (Jupiter, Saturn, Uranus, and Neptune) on the Sun, which causes the Sun to rotate irregularly about the SSB. A minor but still measurable role is exerted by the terrestrial planets (Mercury, Venus, Earth and Mars), while all other objects of the solar system (moons, meteorites, comets, including the Kuiper Belt objects) exerts an almost negligible role.

SIM is physically relevant because it reflects the internal motion of a star's planetary system as a whole. Therefore, the inertial motions of the stars are commonly analyzed to detect the presence and study the characteristics of their planetary systems, the presence of companion stars and black holes, and for other reasons, including further investigation of the nature of the solar dynamo (Perryman & Schulze-Hartung 2011; Butkevich & Lindegren 2014; Cionco & Pavlov 2018).

Regarding the last point, a number of studies have provided empirical evidence for a possible correlation between SIM oscillations and a range of phenomena including solar activity, climate changes and others (e.g., Fairbridge & Shirley 1987; Charvátová 1988, 1995, 2000; Shirley et al. 1990; Zaqarashvili 1997; Landscheidt 1999; Charvátová & Střeštík 2007; Palus et al. 2007; Wilson et al. 2008; Gray et al. 2010; Abreu et al. 2012; Scafetta et al. 2016; Stefani et al. 2019; Scafetta 2020; Scafetta & Bianchini 2022). Some of the most commonly found solar and geophysical oscillations are claimed to have an astronomical origin as such the about 4300 and 1500 yr oscillations (Grootes & Stuiver 1997; Mayewski et al. 1997; Darby et al. 2012); the about 2300 (Bray-Hallstatt) and 1000

(Eddy) year oscillations (Scafetta 2012a; McCracken et al. 2013, 2014; Scafetta et al. 2016); the oscillations found by Suess (1980) and De Vries (1958) (200–250 yr) (see also Sonett & Finney 1990), Jose (1965) (155–185 yr) and Gleissberg (1939) (80–100 yr; other multidecadal oscillations found in the spectral range of 55–65 and 40–50 yr (Ogurtsov et al. 2002; Neff et al. 2001); the well-known 22 yr Hale solar magnetic cycle (Hale et al. 1919) and the 11 yr Schwabe sunspot cycle (Schwabe 1844) that Wolf (1859) claimed to derive from the influence of Venus, Earth, Jupiter and Saturn (see Scafetta 2023). None of these oscillations are observed to be strictly constant; both their periodicities and amplitudes appear to vary with time. The observed variability may simply be due to the fact that each of these astronomical "oscillations" is actually made up of many close frequencies beating together. The theory of a planetary modulation of solar activity changes is still contentious (e.g., Charbonneau 2022; Stefani et al. 2019; Scaffetta 2023; Stefani et al. 2024) also because it may necessitate the existence of some sufficiently strong amplification mechanisms, which, however, may actually exist (Scafetta 2012b; Klevs et al. 2023), or there might be some other still unknown mechanism more directly related to the pulsing structure of the heliosphere (Scafetta et al. 2016).

Here we study the spectral structure of the SIM from 12999 BC to 16998 AD and do not directly address the potential impact of planets on variations in solar activity. However, this research may be indirectly related also to the latter topic because any kind of planetary forcing on the Sun must also be a function of the planetary orbits themselves and, therefore, it must share a number of SIM frequencies since the latter is also a function of the planetary orbits. The above observations suggest that determining the exact spectral structure of the SIM and the physical origin of each spectral peak could have several important physical applications.

In the following, we extract SIM information from 12999 BC to 16998 AD using the most accurate available ephemerides provided by the Solar System Dynamics Group of the Jet Propulsion Laboratory, study their periodograms, and develop a comprehensive planetary frequency model to interpret all observed periodicities.

2. The "Cycles," "Pericycles" and "Apocycles" of the SIM

The positions of the Sun, planets and Moon can be calculated with high accuracy by employing a set of coefficients that are evaluated through the numerical integration of the relevant equations of motion. The Solar System Dynamics Group of the Jet Propulsion Laboratory offers two methods for calculating ephemerides: the Horizons System, accessible at https://ssd.jpl.nasa.gov/horizons/; and a set of coefficient files that can be utilized in compatible software applications, available for download from from ftp://ssd.jpl.nasa.gov/pub/eph/planets/ascii. In this study, we utilize coordinates that are aligned with the International Celestial Reference Frame (ICRF) version 3 (Charlot et al. 2020). The origin of this reference frame is the barycenter of the solar system. The axes are oriented towards distant objects that maintain constant positions in the universe. They are attached, with uncertainty of about 0.1 mas, with the equator and equinox J2000 concerning the Earth.

Based on the Sun's trajectory projections in the ICRF3 x–y plane across the studied period (12999 BC to 16998 AD), quasi-periodic fundamental cycles with a regularity of about 20 yr are clearly present. Two separate phases, each displaying a unique pattern, make up each fundamental cycle. Basic characteristics of the SIM trajectory are depicted in Figure 1. The cyan circles indicate 1 and 2 solar radius; the purple curve indicate the Sun trajectory relative to the barycenter of the solar system, which is in the center; the blue disk represents 1 solar radius.

The Sun travels in a helical loop during the first stage, known as the "pericycle" (PeC) (Figure 1(a)), attaining the least distance and speed in relation to the solar system barycenter (SSB). The trajectory then leaves the loop and begins the second phase, which is called the "apocycle" (ApC) (Figure 1(b)). This stage involves traveling in a wide arc, reaching the greatest distance and speed in relation to the SSB, and ending with the start of the next fundamental cycle (Figure 1(c)). The conjunction-opposition cycle between Jupiter and Saturn is primarily responsible for these two phases. A "pericycle" plus an "apocycle" gives a basic full cycle (C). The term "supercycle" (SpC), which lasts roughly 40 yr, refers to the continuation of two consecutive fundamental cycles. The SIM patterns rotate distinctively in a SpC (Figure 1(d)), producing intricate patterns over time. Seven hundred and fifty-four SpCs are found between 12999 BC and 16998 AD. ApC and PeC trajectories have a propensity to overlap and then align themselves in opposition. Grand Solar minima and other longer oscillations appear correlated with SIM patterns that alternate between more "ordered" and "disordered" trefoil-type motions, which are produced by long SpC sequences (Charvátová 2000; Charvátová & Střeštík 2007; Scafetta et al. 2016).

To better characterize the dynamics of the SIM, we calculated the initial and final dates and approximate path lengths of the SIM trajectory within each specified pericycle, apocycle and cycle. The three types of cycles (PeC, ApC and C) are linked, meaning the end of one trajectory marks the beginning of another. Therefore, identifying the timing of the initial and final points of the pericycles, which are identified by the sequence of nodes highlighted in Figure 1, is sufficient to generate the complete sequence of PeC, ApC and C. The computer algorithm search for each cycle the node as the entry and exit points of the pericycles, which are the two points of the cycle with the shortest distance between them. This approach allowed us to determine the positions of these two points. The calculation uses a 1 s time step. For an approximate

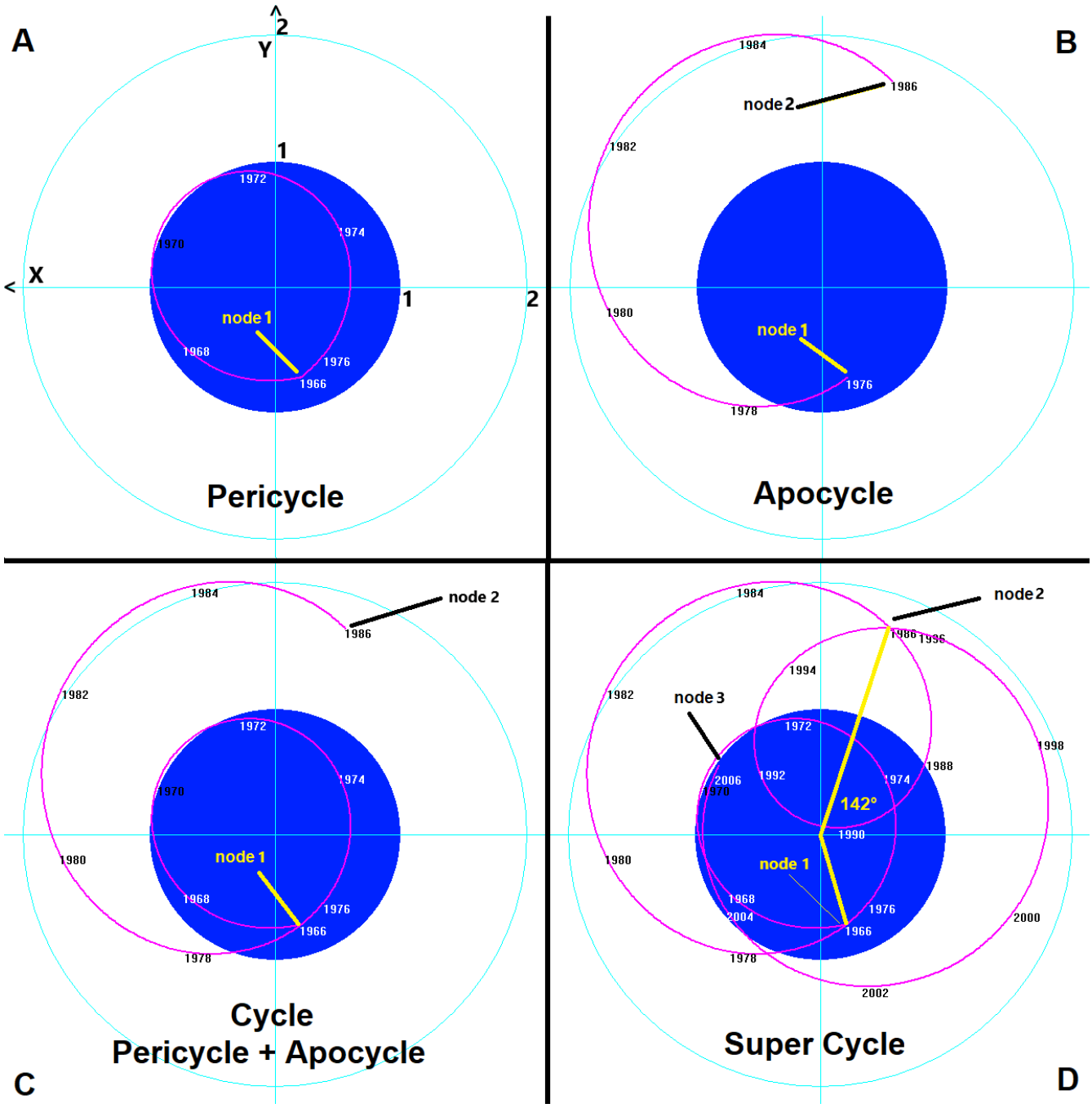

Figure 1. Example of orbits of the Sun relative to the center of mass of the solar system. Reference frame: Ecliptic of J2000. (A) Pericycle; (B) Apocycle; (C) The pericycle-apocycle trajectory composing a "cycle;" (D) Supercycle 378 (years 1965–2006) with its rotation of 142° between the nodes. The blue disk indicates 1 solar radius. The cyan circles indicate distances of 1 and 2 solar radii from the center; the purple curves indicate the Sun trajectory.

calculation of the path lengths, we used another program to divide the pericycle curves into small arcs, each spanning one-hundredth of a Julian day. Using this kinematic approximation, we arrived at our results through cumulative path summations. Figure 2 depicts the sequences of path length and periods for the pericycles, apocycles, and basic cycles.

This study aims to explicitly examine and model the spectral structure of records pertaining to the duration and length of the "cycles," "pericycles," and "apocycles" of the SIM. Figure 2 illustrates the six records of all pericycles, apocycles, and cycles spanning the period from 12999 BC to 16998 AD. The figure demonstrate that the SIM orbits are characterized by complex

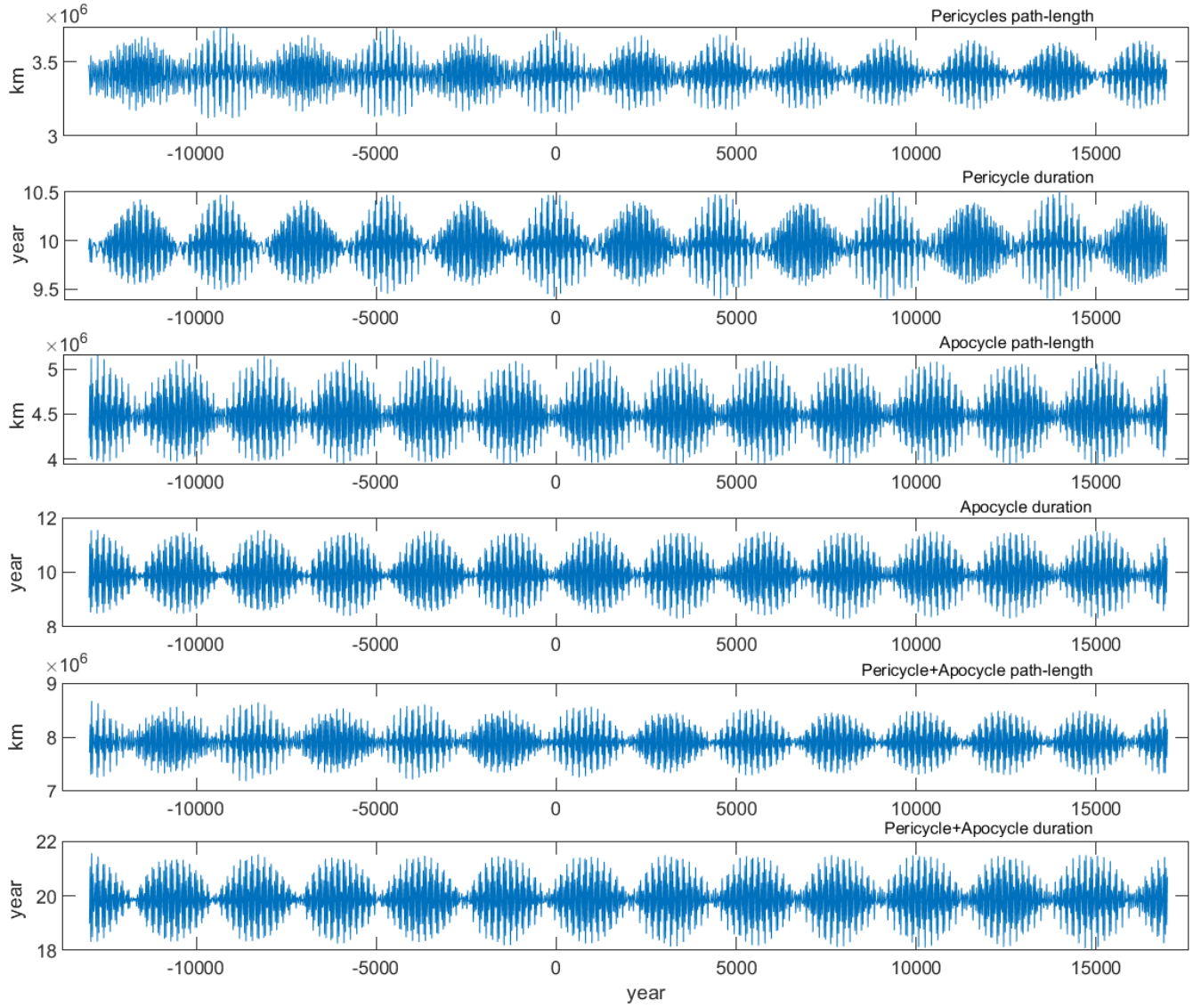

Figure 2. Pericycle, Apocycle and Cycle duration and length. Major beats at the Bray-Hallstatt period of 2318 yr are evident. See "data availability" section.

beats occurring at multiple frequencies. The most evident one has a periodicity of approximately 2318 yr, which corresponds to the Bray-Hallstatt oscillation observed in several solar and climate records (McCracken et al. 2013, 2014; Scafetta et al. 2016; Scafetta 2020). The Lomb-Scargle periodograms of the six records are presented in Figure 3 and, as expected, present a large number of spectral peaks whose planetary origin is now modeled. These periodograms are significantly sharper than those obtained in the literature (e.g., Jakubcová & Pick 1986; Cionco & Pavlov 2018) because based on 30,000 yr of data. Note that the periodogram is a continuous function of the frequency and must be preferred to the Fast Fourier Transform (FFT) because the latter provides only a discrete power spectrum, which could not capture well the low-frequency components of the signal.

3. Modeling the Spectral Structures of the SIM

It is hypothesized that the intricate SIM dynamics derives from trigonometric series of the orbital periodicities of the planets and their mutual alignments and beats. Consequently, the modeling of this dynamics can be effectively achieved by generalizing the concept of orbital near-commensurabilities as proposed by Goldreich & Sciama (1965) and the "orbital invariant inequality" model by Scafetta (2020) in the following way.

If P_1 and P_2 are the orbital period of two planets, their conjunction or synodic period P_{12} or frequency f_{12} is

$$\frac{1}{P_{12}} = \left| \frac{1}{P_1} - \frac{1}{P_2} \right| = |f_1 - f_2| = f_{12}, \qquad (1)$$

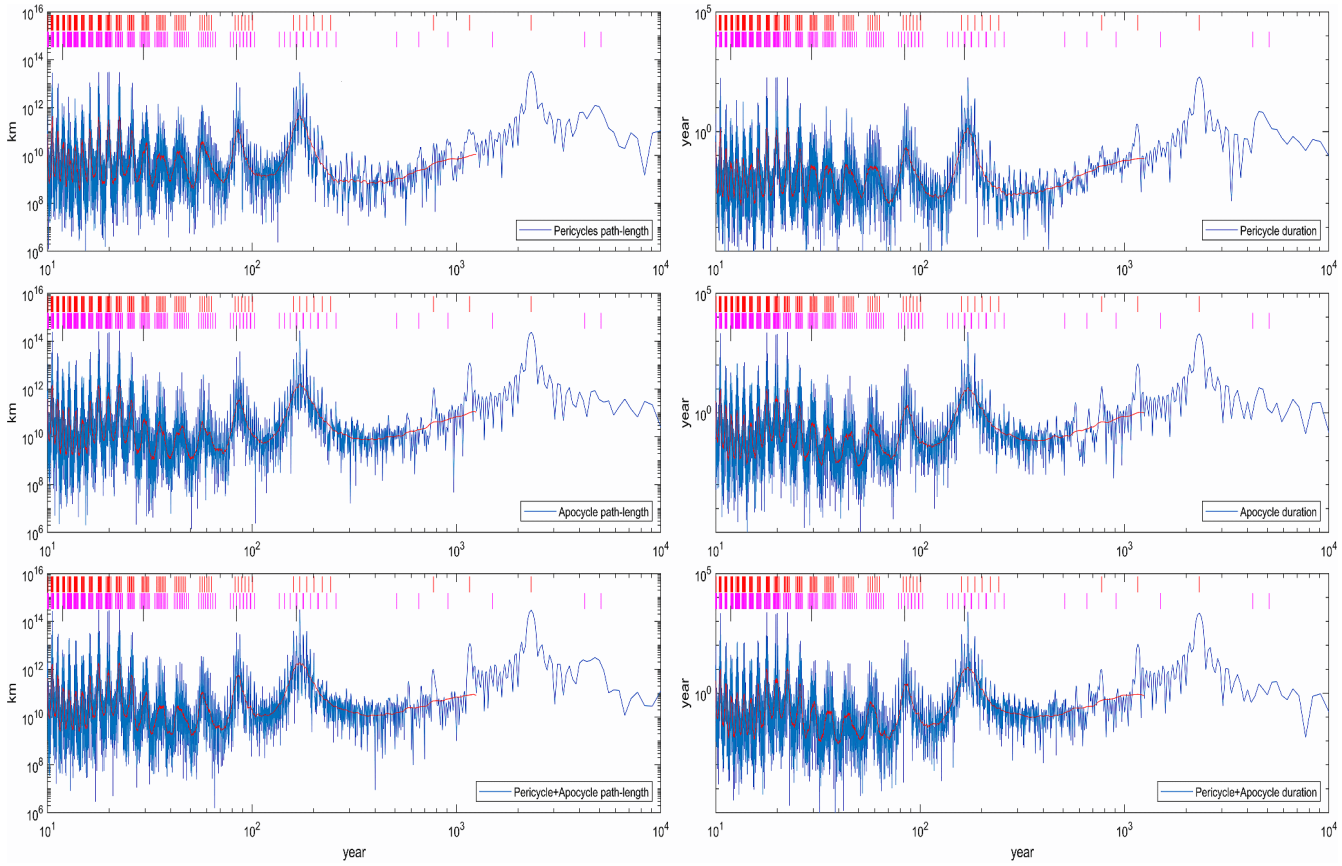

Figure 3. Lomb–Scargle periodograms of the records shown in Figure 2. The red vertical segments are the orbital invariant inequalities among Jupiter, Saturn, Uranus and Neptune with order $M \leqslant 5$ as discussed in Scafetta (2020). The purple vertical segments are the beats among the orbital period of one planet (e.g., Jupiter) and the orbital invariant inequalities among Jupiter, Saturn, Uranus and Neptune with order $M \leqslant 5$. The four black vertical segments correspond to the orbital periods of Jupiter (11.86 yr), Saturn (29.46 yr), Uranus (84.01 yr) and Neptune (164.8 yr). For the orbital inequality periods, see "data availability" section.

while their spring tidal period is

$$\frac{1}{T_{12}} = 2\left|\frac{1}{P_1} - \frac{1}{P_2}\right| = 2|f_1 - f_2|, \tag{2}$$

For n planets with periods P_i, and $i = 1, 2, \ldots, n$, Equation (1) can be generalized by defining the periods

$$\frac{1}{P_{a_1,a_2,\ldots,a_n}} = \left|\sum_{i=1}^{n} \frac{a_i}{P_i}\right| = \left|\sum_{i=1}^{n} a_i \cdot f_i\right|, \tag{3}$$

where a_i are (positive or negative) integers. We label the near-commensurability periodicities expressed by Equation (3) as "orbital inequalities" as a generalization of the Great Inequality concept among the periods of Jupiter and Saturn extensively studied by Kepler and Laplace (Willson 1985).

Scafetta (2020) demonstrated that among all possible orbital inequalities (Equation (3)) there is a special subgroup that is defined by the additional condition

$$\sum_{i=1}^{n} a_i = 0. \tag{4}$$

Equation (4) implies that Equation (3) can be decomposed as a sum of pairs of synodic cycles of the type of Equation (1). Consequently, they are the synodic periods P_{ij} of pairs of planets plus their combined beats and harmonics. This subgroup was labeled "orbital invariant inequalities" because its periods are invariant relative to any rotating reference system. In fact, a set of planets $i = 1, 2, \ldots, N$ with orbital period P_i observed from a reference system spinning with a period P centered in the Sun, are seen to orbit with periods $P_i^{'}$ given by

$$\frac{1}{P_i^{'}} = \frac{1}{P_i} - \frac{1}{P}. \tag{5}$$

Thus, using Equation (4), the orbital inequality $P^{'}_{a_1,a_2,\ldots,a_n}$ relative to such a rotating reference system is given by the

following equation:

$$\frac{1}{P'_{a_{1\ldots n}}} = \left| \sum_{i=1}^{n} \frac{a_i}{P'_i} \right| = \left| \sum_{i=1}^{n} \frac{a_i}{P_i} - \frac{\sum_{i=1}^{n} a_i}{P} \right| = \left| \sum_{i=1}^{n} \frac{a_i}{P_i} \right| = \frac{1}{P_{a_{1\ldots n}}}, \quad (6)$$

which means that $P'_{a_{1\ldots n}} = P_{a_{1\ldots n}}$. Because of this property, Scafetta (2020) proposed that the frequencies of the "orbital invariant inequalities" may play a pivotal role in triggering gravitational synchronization mechanisms within the solar system and the Sun, both of which are rotating systems.

The proposed vectorial representation of the invariant inequalities significantly simplifies the calculations and the interpretation of each periodicity. To illustrate the case, Figure 1 reports the sidereal orbital periods published by the "NASA Planetary Fact Sheet—Metric" of Jupiter ($P_J = 11.86224$ yr), Saturn ($P_S = 29.45778$ yr), Uranus ($P_U = 84.01389$ yr) and Neptune ($P_N = 164.792$ yr). The sidereal orbital periods are necessary for evaluating the synodic periods between pairs of planets. These four periods can be represented by the vector (1, 0, 0, 0), (0, 1, 0, 0), (0, 0, 1, 0), (0, 0, 0, 1), respectively. Thus, the synodic frequency of Jupiter and Saturn can be represented as (1, −1, 0, 0) = (1, 0, 0, 0) − (0, 1, 0, 0), i.e., as the difference between the vectors (1, 0, 0, 0) and (0, 1, 0, 0). Similarly, the synodic frequency of Uranus and Neptune is represented by the vector (0, 0, 1, −1) = (0, 0, 1, 0) − (0, 0, 0, 1), i.e., the difference between the vectors (0, 0, 1, 0) and (0, 0, 0, 1). The tidal frequency is twice the synodic frequency and, in the case of Jupiter and Saturn, can be represented by the vector 2(1, −1, 0, 0) = (2, −2, 0, 0), which is the first harmonic of the synodic frequency. This notation can be extended naturally to the nth order of harmonics as the vector n(1, −1, 0, 0). Moreover, for example, (1, −1, −1, 1) = (1, −1, 0, 0) − (0, 0, 1, −1), which means that (1, −1, −1, 1) represents the beat frequency between the synodic frequencies Jupiter–Saturn and Uranus–Neptune. Similarly, all "orbital invariant inequalities" can be decomposed as beats of several orders of synodic periods of planetary pairs. For instance, Scafetta et al. (2016) and Scafetta (2020) demonstrated that the orbital invariant inequality (1, −3, 1, 1)—which corresponds to the Bray-Hallstatt period of 2318 yr—can be decomposed in two terms as [(1, −1, 0, 0) − (0, 1, −1, 0)] − (0, 1, 0, −1), where the first corresponds to the beat between the synodic periods Jupiter–Saturn (1, −1, 0, 0) and Saturn–Uranus (0, 1, −1, 0), and the second corresponds to the synodic period Saturn–Neptune (0, 1, 0, −1).

The "orbital invariant inequalities" can be classified by defining two order parameters: $M = \max|a_i|$ and $K = \frac{1}{2}\sum|a_i|$ for $i = 1, 2, \ldots, n$. It can be expected that the smaller the order, the more relevant the periodicity may be. The order K indicates the number of synodic periods or planetary pairs that are in phase with one another. To illustrate, the aforementioned Bray-Hallstatt frequency (1, −3, 1, 1) has $K = 3$, indicating that this frequency is generated by three planetary synodic periods, as demonstrated above.

A limitation of the "orbital invariant inequality" model is that it assumes circular orbits, whereas the actual orbits are elliptical. Consequently, the distance between a planet and the Sun varies from a minimum (perihelion) to a maximum (aphelion). Therefore, any physical function of the planetary orbits should depend not only on the orbital invariant inequalities, i.e., the synodic planetary periods, but also on the actual orbital periods.

For example, the Great Inequality between Jupiter and Saturn has been traditionally understood as derived from the fact that five times the period of Jupiter is nearly twice the period of Saturn and that, therefore, it could be represented by the vector (−2, 5), which corresponds to $P_{(-2,5)} = [-2/P_J + 5/P_S]^{-1} = 883$ yr (Willson 1985); the vector (−2, 5) = 3(0, 1) − 2(1, −1) and, therefore, can be also interpreted as a beat period or inequality between the third harmonic of Saturn's period and the spring tidal period between Jupiter and Saturn.

To solve the problem, we propose a new "extended orbital invariant inequality" model as

$$\frac{1}{P_{a_1,\ldots,a_j+b,\ldots,a_n}} = \left| \left(\sum_{i=1}^{n} \frac{a_i}{P_i} \right) + \frac{b}{P_j} \right|, \quad (7)$$

where $\sum a_i = 0$, b is a positive or negative integer, and P_j is the actual period of the jth planet. If $b = 0$, $P_{a_1,\ldots,a_j+b,\ldots,a_n} = P_{a_1,\ldots,a_j,\ldots,a_n}$, which is an orbital invariant inequality, if all coefficient $a_i = 0$, $P_{a_1,\ldots,a_j-b,\ldots,a_n}$ is the bth harmonic of the orbital period of the jth planet. In all other cases, $P_{a_1,\ldots,a_j+b,\ldots,a_n}$ is the beat frequency between the invariant inequality $P_{a_1,a_2,\ldots,a_n}$ and the bth harmonic of the orbital frequency of the jth planet. The period $P_{a_1,\ldots,a_j+b,\ldots,a_n}$ is well represented by the integer vector $(a_1, \ldots, a_j + b, \ldots, a_n)$.

Equation (7) exhibits a noteworthy mathematical attribute. Indeed, the addition of a second planet to the equation is not necessary, as all the frequencies of interest can be adequately represented by even a single planet. It is possible to substitute one planet for another or to combine orbital periods through the simple rearrangement of the adopted orbital invariant inequalities. To illustrate, let us assume that $j = 1$ (e.g., by using Jupiter) and that Equation (7) is represented by the vector $(a_1 + b, a_2, a_3, a_4) = (a_1, a_2, a_3, a_4) + (b, 0, 0, 0)$,

where the first term represents an orbital invariant inequality, as its coefficients satisfy the condition of Equation (4), while the second term corresponds to the bth harmonic of the orbital period of Jupiter. However, the same vector can also be expressed as $(a_1 + b, a_2, a_3, a_4) = (a_1 + b, a_2 - b, a_3, a_4) + (0, b, 0, 0)$, where the first term again represents an orbital invariant inequality, as its coefficients satisfy the condition of Equation (4), while the second term corresponds to the bth harmonic of the period of Saturn. This property can be readily extended to any other planet. Consequently, all periodicities can be obtained by incorporating a single additional orbit, as illustrated by the following equation:

$$\frac{1}{P_{a_1-1,a_2,\ldots,a_n}} = \left| \left(\sum_{i=1}^{n} \frac{a_i}{P_i} \right) - \frac{1}{P_1} \right|. \quad (8)$$

In this model, the period of Jupiter, represented by the symbol P_1, is the fundamental parameter. Extensions of this model incorporating multiple planetary harmonics can be constructed in a similar manner; however, for the purposes of this investigation, we focus solely on the frequency generated by the basic orbital periods ($b = 1$), which are the most relevant.

Figures 3 (in function of the period) and Equation (4) (in function of the frequency) demonstrate that the "extended orbital invariant inequality" model derived from Equation (7) can reproduce the numerous visible spectral peaks and their clustered structure. The representative frequency samples of the model are depicted by the black, red and purple segments at the top of each periodogram. The resolution of the periodogram is determined by the length of the data sequence, which is about $T = 30{,}000$ yr. Thus, the smallest resolvable frequency difference is approximately $\Delta f = 1/T = 0.0000333$, and for a period P the error is a function of the period itself as

$$\Delta P = P^2 \Delta f = \frac{P^2}{T}. \quad (9)$$

This equation gives an idea of the precision to which one can estimate the frequency and the period from the periodogram.

We notice that, in this context, direct periodogram analysis with associated uncertainties is preferred over alternative methodologies that progressively remove the most relevant harmonics detected in the periodogram to identify whether any remaining signal remains after detrending, as such an approach requires regression analysis and is here impractical due to the extremely large number and of the high spectral density of the analyzed harmonics.

The four black vertical segments in Figures 3 and 4 correspond to the orbital periods of Jupiter, Saturn, Uranus, and Neptune. The red vertical segments represent the orbital invariant inequalities (a_1, a_2, a_3, a_4) among Jupiter, Saturn, Uranus and Neptune with order $M \leqslant 5$ (see Scafetta 2020). The purple vertical segments represent the beats between the orbital period of a given planet (e.g., Jupiter) and the orbital invariant inequalities among Jupiter, Saturn, Uranus, and Neptune with order $M \leqslant 5$. These periodicities are represented by the vectors $(a_1 - 1, a_2, a_3, a_4)$. Table 2 presents the orbital invariant inequalities with a period exceeding 40 yr, other frequencies are listed in the Supplementary table.

Table 1
Orbital Parameters from NASA Planetary Fact Sheet—Metric (https://web.archive.org/web/20240614155913/https://nssdc.gsfc.nasa.gov/planetary/factsheet/, Retrieved 2024 June 14)

	Sidereal Orbital Period	
	(days)	(yr)
Earth	365.256 ± 0.005	1.00004 ± 0.002
Jupiter	4332.589 ± 0.005	11.8622 ± 0.0002
Saturn	10759.22 ± 0.05	29.4578 ± 0.0004
Uranus	30685.4 ± 0.5	84.014 ± 0.002
Neptune	60189.0 ± 0.5	164.792 ± 0.003

Note. The year is defined from the tropical period of the Earth, which is 365.242 ± 0.005 days. The error bars are hypothesized assuming uncertain only at the last available digit.

Figures 3 and 4 demonstrate that the reported theoretical periods derived from the aforementioned "extended orbital invariant inequality" model tend to align with the spectral peaks of the SIM sequences referring to the length and periods of the "cycles," "pericycles," and "apocycles." This correspondence can be easily observed for the low frequencies. Small discrepancies could be explained with the fact that the planetary periods used to calculate the modeled frequencies (Table 1) may not exactly correspond to the periods implicit in the adopted Ephemeris and to some computational error. Figure 3 collects a very large number of frequencies and the simplest way to verify the correspondence of the spectral peaks with the periods predicted by the model is by visual inspection by zooming the figure. In any case, Table 2 also lists the main periods derived from the peaks observed in the periodograms shown in Figure 3 and they well correspond to the periods derived from the proposed model within their spectral uncertainty.

By increasing the order M, additional frequencies can be obtained from the model, but the good correspondence between the depicted frequency cluster with the top portion of the periodogram lobes depicted in Figure 3 suggest that small values of the order M are typically associated with the harmonics with the relative higher power for each lobe.

Additionally, the most prominent spectral peaks of the SIM are found to originate from the orbital periods of the four Jovian planets. Figure 3 shows a strong harmonic around 2318 yr, known as the Bray-Halstatt cycle. This periodicity is

Table 2
Full list of Invariant Inequalities: Period $P \geqslant 40$ yr and $M \leqslant 5$

Orbital Invariant Inequalities (Equations (3) and (4))					Their Beats with Jupiter		
(Jup, Sat, Ura, Nep)	(M, K)	P_{model} (year)	$P_{\text{Periodogram}}$ (year)	cluster	(Jup -1, Sat, Ura, Nep)	P_{model} (year)	$P_{\text{Periodogram}}$ (year)
(1, −3, 5, −3)	(5, 6)	42.069 ± 0.002	42.08 ± 0.06		(0–1, 3, −2, −1)	81.072 ± 0.004	81.2 ± 0.25
(0, 0, 4, −4)	(4, 4)	42.847 ± 0.002	42.86 ± 0.06		(2–1, −3, 4, −3)	84.265 ± 0.007	84.1 ± 0.25
(2, −5, 1, 2)	(5, 5)	43.653 ± 0.002	43.65 ± 0.06		(2–1, −3, 0, 1)	87.171 ± 0.004	87.3 ± 0.25
(1, −3, −3, 5)	(5, 6)	43.654 ± 0.002	43.65 ± 0.06	∼45 yr	(1–1, 0, 3, −4)	87.445 ± 0.005	87.3 ± 0.25
(1, −2, 0, 1)	(2, 2)	44.591 ± 0.001	44.58 ± 0.07		(0–1, 2, 3, −5)	90.575 ± 0.006	90.8 ± 0.3
(0, 1, −1, 0)	(1, 1)	45.362 ± 0.001	45.37 ± 0.07		(3–1, −5, 0, 2)	90.870 ± 0.007	90.8 ± 0.3
(1, −4, 2, 1)	(4, 4)	46.268 ± 0.002	46.27 ± 0.07		(0–1, 3, 2, −5)	90.873 ± 0.006	90.8 ± 0.3
(1, −1, −5, 5)	(5, 6)	47.209 ± 0.002	47.21 ± 0.08		(1–1, −1, 4, −4)	94.259 ± 0.007	94.5 ± 0.3
(1, −3, 4, −2)	(4, 5)	55.754 ± 0.003	55.71 ± 0.1		(2–1, −2, −1, 1)	94.579 ± 0.004	94.5 ± 0.3
(0, 0, 3, −3)	(3, 3)	57.129 ± 0.003	57.14 ± 0.1		(2–1, −4, 5, −3)	98.25 ± 0.01	98.5 ± 0.4
(2, −5, 0, 3)	(5, 5)	58.571 ± 0.003	58.55 ± 0.1		(1–1, 1, −2, 0)	98.603 ± 0.004	98.5 ± 0.4
(1, −3, −2, 4)	(4, 5)	58.573 ± 0.003	58.55 ± 0.1	∼60 yr	(0–1, 4, −3, −1)	102.98 ± 0.01	103.1 ± 0.4
(1, −2, −1, 2)	(2, 3)	60.090 ± 0.003	60.1 ± 0.15		(1–1, 1, −5, 3)	135.82 ± 0.02	135.3 ± 0.6
(0, 1, −2, 1)	(2, 2)	61.690 ± 0.003	61.7 ± 0.15		(2–1, −2, −4, 4)	144.28 ± 0.02	144.5 ± 0.7
(1, −4, 3, 0)	(4, 4)	63.377 ± 0.004	63.3 ± 0.15		(0–1, 3, −1, −2)	153.85 ± 0.02	154.1 ± 0.8
(1, −3, 3, −1)	(3, 4)	82.638 ± 0.005	82.6 ± 0.25		(3–1, −5, −3, 5)	153.86 ± 0.03	154.1 ± 0.8
(0, 0, 2, −2)	(2, 2)	85.693 ± 0.005	85.7 ± 0.25		(2–1, −3, 3, −2)	165.77 ± 0.02	165.3 ± 0.9
(2, −5, −1, 4)	(5, 6)	88.981 ± 0.007	89.0 ± 0.3		(2–1, −3, 1, 0)	177.40 ± 0.02	177.6 ± 1.0
(1, −3, − 1, 3)	(3, 4)	88.984 ± 0.005	89.0 ± 0.3	Gleissberg	(1–1, 0, 2, −3)	178.54 ± 0.02	177.6 ± 1.0
(1, −2, −2, 3)	(3, 4)	92.533 ± 0.005	92.5 ± 0.3		(3–1, −5, −1, 3)	193.43 ± 0.04	192.7 ± 1.3
(0, 1, −3, 2)	(3, 3)	96.382 ± 0.006	96.4 ± 0.4		(0–1, 3, 1, −4)	193.44 ± 0.02	192.7 ± 1.3
(1, −4, 4, −1)	(4, 5)	100.56 ± 0.01	100.7 ± 0.5		(1–1, −1, 5, −5)	209.45 ± 0.05	209.6 ± 1.5
(1, −3, 2, 0)	(3, 3)	159.585 ± 0.02	159.7 ± 1.0		(2–1, −2, −2, 2)	211.04 ± 0.02	212 ± 1.5
(0, 0, 1, −1)	(1, 1)	171.39 ± 0.01	171.5 ± 1.0	Jose	(1–1, 1, −3, 1)	232.18 ± 0.04	231 ± 2
(2, −5, −2, 5)	(5, 7)	185.06 ± 0.03	185 ± 1.2		(0–1, 4, −4, 0)	258.04 ± 0.07	258 ± 2
(1, −3, 0, 2)	(3, 3)	185.07 ± 0.02	185 ± 1.2		(0–1, 4, −5, 1)	510.4 ± 0.3	513 ± 10
(1, −2, −3, 4)	(4, 5)	201.12 ± 0.03	201 ± 1.5		(1 −1, 1, −4, 2)	654.5 ± 0.4	671 ± 15
(0, 1, −4, 3)	(4, 4)	220.23 ± 0.04	220 ± 2.0	Suess-de Vries	(2 −1, −2, −3, 3)	912.1 ± 0.6	925 ± 30
(1, −4, 5, −2)	(5, 6)	243.36 ± 0.07	243 ± 2.0		(0 −1, 3, 0, −3)	1503 ± 2	1470 ± 80
(0, 1, −5, 4)	(5, 5)	772.7 ± 0.6	781 ± 20	Eddy	(3 −1, −5, −2, 4)	1504 ± 2	1470 ± 80
(1, −2, −4, 5)	(5, 6)	1159 ± 2	1149 ± 44		(1 −1, 0, 1, −2)	4279 ± 4	4167 ± 700
(1, −3, 1, 1)	(3, 3)	2318 ± 3	2326 ± 180	Bray-Hallstatt	(2 −1, −3, 2, −1)	5056 ± 16	5000 ± 700

Note. The left columns show the most longer periods of the beats of Jupiter with the invariant inequality period $P \geqslant 40$ yr and $M \leqslant 5$. For the full orbital inequality data up to cluster #21, see "data availability" section. The error bars are derived from the hypothesized errors reported in Table 1. The periods $P_{\text{Periodogram}}$ are deduced from the periodograms depicted in Figure 3 with error bars given by $\Delta P = P^2/30{,}000$.

spectrally coherent with the orbital invariant inequality (1, −3, 1, 1), as reported in Table 2. Scafetta (2020) demonstrated that this periodicity derives from (1, −3, 1, 1) = [(1, −1, 0, 0) − (0, 1, −1, 0)] − (0, 1, 0, −1), namely, it is the beat period between the beat period between the Jupiter–Saturn synodic cycle and the Saturn–Uranus synodic cycle, and the Suturn–Neptune synodic cycle. Figure 3 also suggests the existence of two weak harmonics with periods around 4279 yr and 5056 yr, which result from (1 −1, 0, 1, −2) = (0, 0, 1, −2) = (0, 0, 1, −1) − (0, 0, 0, 1), and (2 −1, −3, 2, −1) = (1, −3, 2, −1) = (1, −1, 0, 0) − 2 (0, 1, −1, 0) − (0, 0, 0, 1), as reported in Table 2. The first harmonic can be attributed to the beat between the Uranus–Neptune synodic periodicity, (0, 0, 1, −1), and the orbital period of Neptune, (0, 0, 0, 1), and the second derives from a combined beat between the Jupiter-Saturn synodic period, the Saturn–Uranus tidal period and the orbit of Neptune.

Scafetta (2012b) and Scafetta & Bianchini (2022) discussed another significant example: the orbital invariant inequality (3, −5, 2) between Venus, Earth and Jupiter, which produces a period of 11.07 yr, which appears to be roughly synchronized with the timing of the sunspot cycle (see: Stefani et al. 2019, 2024; Scaffetta 2023). Since (3, −5, 2) = 3(1, −1, 0) − 2(0, 1, −1), this harmonic can be interpreted as a beat between the third harmonic

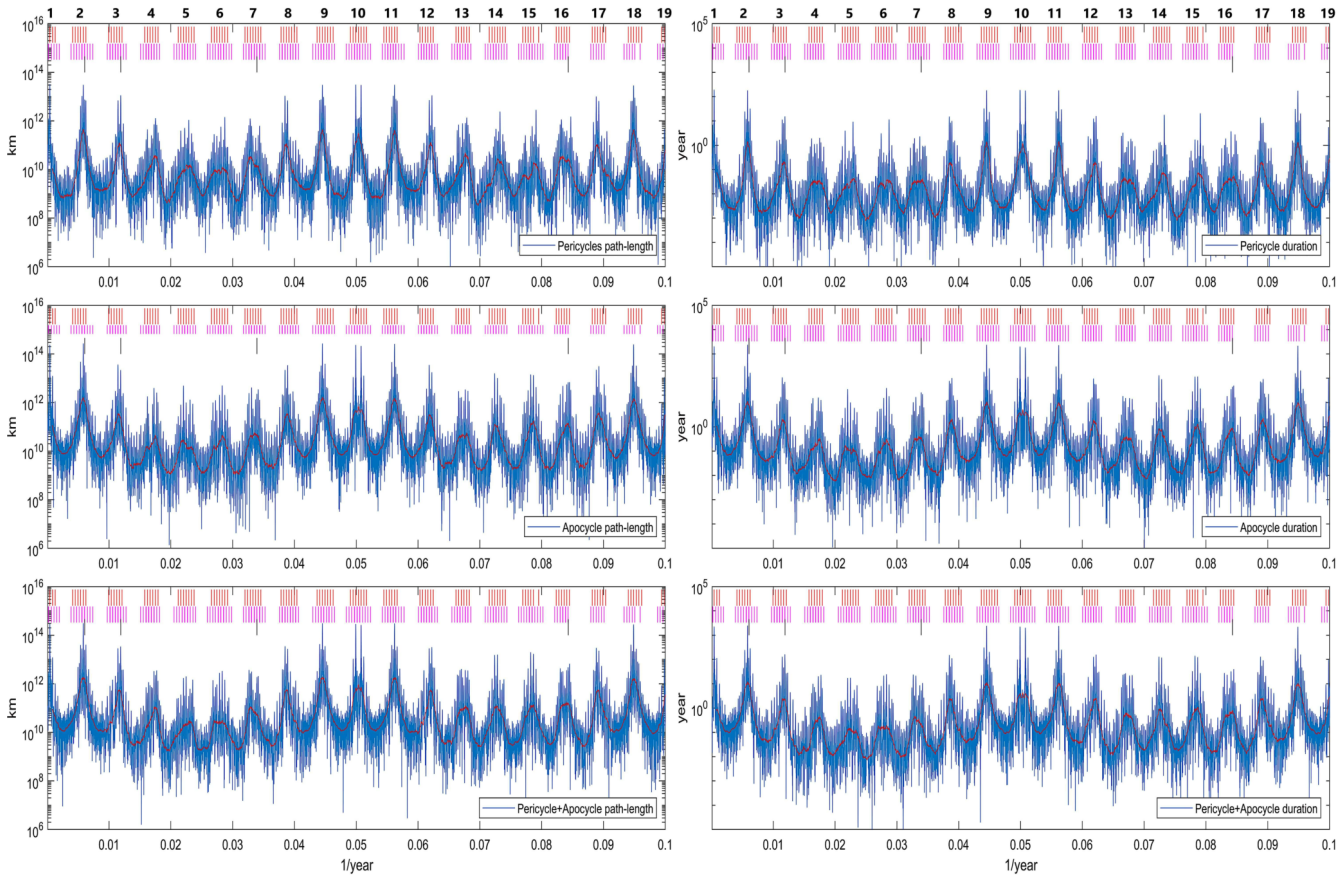

Figure 4. The same as Figure 3, but in function of the frequency. The top lists the clusters from #1 to #19.

Table 3
Cluster of the periodicities depited in Figure 3

cluster	Average (yr)		Period-range (yr)		Equation (9)
#	Arithmetic	Logarithmic	Model Cluster	Periodogram Lobe	$179/(n-1)$.
1	2783	1606	510.4–5056	300–30,000(?)	N/A
2	197	187	135.8–258.0	120–300	179 ± 10.00
3	90.7	89.8	78.34–103.0	71–120	89.50 ± 5.00
4	60.6	60.3	55.04–66.17	51–71	59.67 ± 3.33
5	45.2	45.1	41.66–48.74	40–51	44.75 ± 2.50
6	36.1	36.0	33.51–38.58	32.5–40	35.80 ± 2.00
7	30.0	29.9	28.38–31.49	27.6–32.5	29.83 ± 1.67
8	25.6	25.6	24.60–26.60	23.8–27.6	25.57 ± 1.43
9	22.4	22.4	21.52–23.26	21.2–23.8	22.37 ± 1.25
10	19.89	19.87	19.12–20.66	18.7–21.2	19.89 ± 1.11
11	17.89	17.88	17.33 –18.44	17.0–18.7	17.90 ± 1.00
12	16.25	16.24	15.84–16.65	15.5–17.0	16.27 ± 0.91
13	14.94	14.93	14.59–15.27	14.3–15.5	14.92 ± 0.83
14	13.78	13.78	13.45–14.11	13.2–14.3	13.77 ± 0.77
15	12.79	12.79	12.47–13.11	12.3–13.2	12.79 ± 0.71
16	12.02	12.02	11.83–12.18	11.55–12.3	11.93 ± 0.67
17	11.24	11.23	11.07–11.37	10.86–11.55	11.19 ± 0.63
18	10.57	10.56	10.40–10.71	10.25–10.86	10.53 ± 0.59
19	9.967	9.966	9.804–10.13	9.64–10.25	9.94 ± 0.56
20	9.475	9.474	9.348–9.601	9.17–9.64	8.94 ± 0.53

Note. "Average" indicates the average among the modeled frequencies of the clusters reported in Table 2 and in the Supplementary, "Period-range" indicates their range between the lowest and higher frequencies listed in each cluster. "Periodogram lobe" indicates the ranges of each lobe present in the periodograms depicted Figures 3 and 4 estimated from the minima of the red smooth curves.

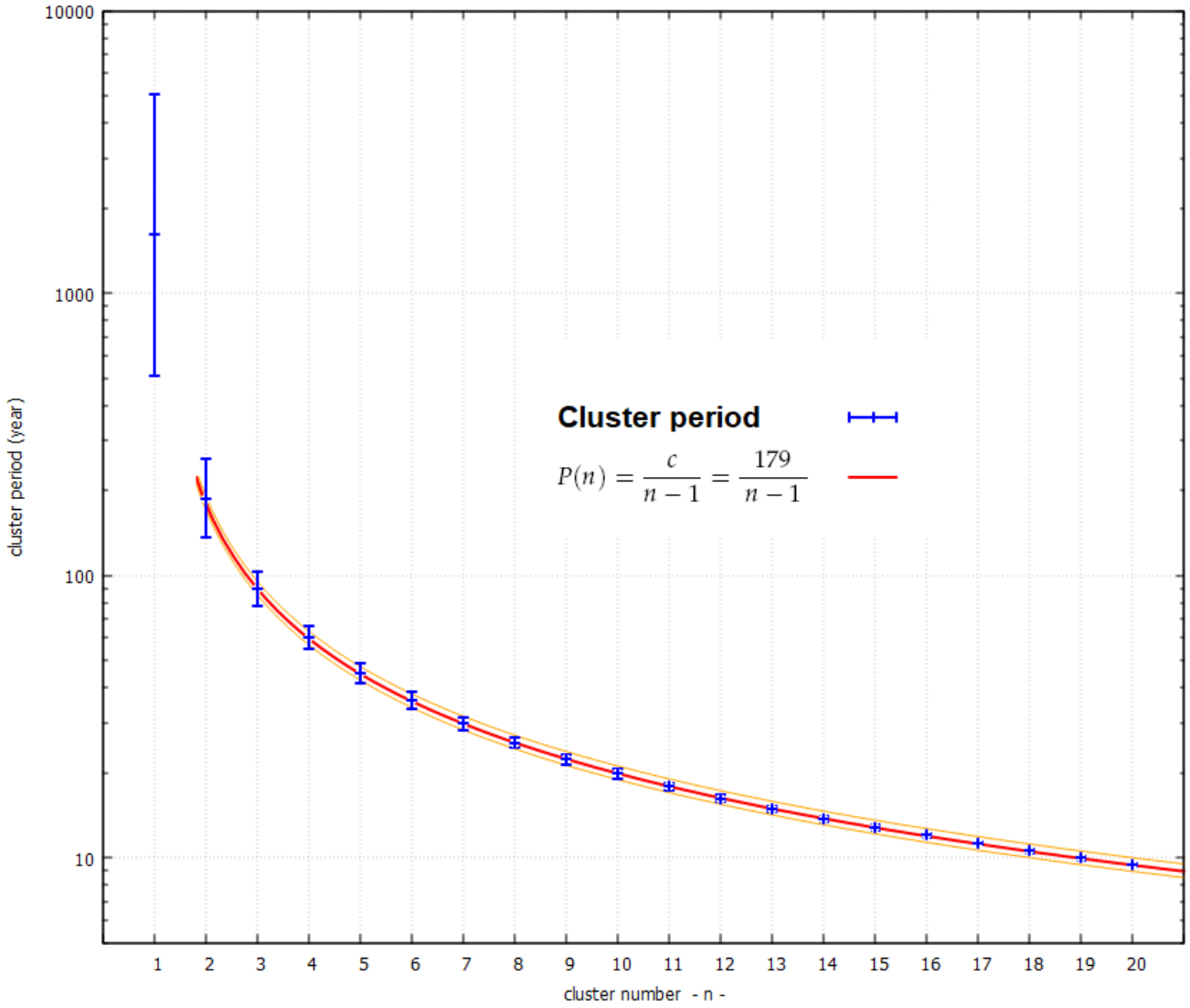

Figure 5. Spectral structure of the SIM: the period ranges of the clusters of the SIM listed in Table 3 and in the more extended Table of the Supplementary. The data are fitted with Equation (10)

of the Venus–Earth synodic period and the second harmonic of the Earth–Jupiter synodic period, which is the Earth–Jupiter spring tidal period.

Finally, since the phases of the orbital and synodic cycles can be determined with a good precision, each orbital periodicity derived from any Equation (8) can be associated with a finite number possible phases derived from a combination of the phases of the synodic cycles of planetary pairs. Examples of phase determinations regarding the two above orbital invariant inequalities are discussed in Scafetta (2020), Scafetta & Bianchini (2022). Possible uncertainties derive from the fact that the orbits are not perfectly circular nor perfectly constant.

Figures 3 and 4 illustrate that the periodograms of the SIM and the periodicities derived from the orbital inequalities are not randomly distributed; rather, they form a sequence of specific frequency clusters, which can be approximately identified by the large lobes of enhanced power in the periodograms. These lobes are better identified by the red smooth periodogram curves, whose minima could be used to constrain each cluster. Table 3 reports also the period range of each periodogram lobe, which can be used to define each cluster. Figure 4 shows that the frequency lobes also form a harmonic scale and can be numbered. There are about 18 lobes in a frequency range of 0.1 1/yr, which correspond to a frequency band of about 0.056 1/yr, that is a period of about 179 yr. Thus, the edges of each cluster may be defined by the minimum of the smooth periodograms. Figures 3 and 4 highlight the existence of bands of higher spectral power for

periods above 80 yr and for periods around 20 yr, that is between 17 and 23 yr or frequencies 0.043 1/yr and 0.058 1/yr.

The top 20 clusters, with their respective period ranges calculated from the evaluated frequencies reported in Table 2 and in the longer Table reported in the Supplementary, are presented in Table 3 for the interval between 10 and 10,000 yr. Figure 5 depicts these clusters as a function of their harmonic number. The periods can be well fitted for the clusters $n = 2$–20 with the function

$$P_n = \frac{1}{F_n} = \frac{c}{n-1} = \frac{179}{n-1}\ \text{yr}, \tag{10}$$

where n is the cluster number as listed in Table 3. The coefficient c varies between 170 (using the minima of the period range of the clusters) and 190 (using the maxima of the period range of the clusters), with a best fit of $c \approx 179$ (using the logarithmic scale). It can be observed that 179 yr is approximately the average duration of the hypercycles.

Equation (10) was conjectured and discussed in other works such as by Jakubcová & Pick (1986), Scafetta (2014, Equation (8)) and Scafetta & Bianchini (2022, Equation (3)). However, these authors analyzed a significant shorter SIM record that the one here analyzed (about 30,000 yr) and could not identify several frequency clusters. On the contrary, Figure 5 shows the presence of at least 20 consecutive frequency clusters, which provides the best validation of Equation (9) to date.

The 179 yr period corresponds to the period indicated by Jose (1965). Table 2 demonstrates that this period does not represent a single periodicity, but an entire cluster of planetary frequencies, which Table 2 labels "Jose cluster" and which is made by at least 5 major planetary harmonics, but many others are visible in Figure 3. Equation (9) is unable to capture the cluster $n = 1$, which includes the Eddy and Bray-Hallstatt cycles, due to the divergence of the function to infinity.

It is important to highlight that using ephemerides with shorter time spans than the approximately 30,000 yr provided by the latest JPL ephemeris files (DE441) results in greater uncertainties and may fail to detect several theoretical frequencies, in addition to the very low-frequency components. For instance, DE422 covers a total epoch of about 6000 yr (from https://ssd.jpl.nasa.gov/planets/eph_export.html, accessed on 2025 April 18), leading to spectral errors, which can be calculated using Equation (9), five times larger than those obtained with DE441. These substantial errors would significantly hinder the identification of various close harmonics predicted by the model and listed in Table 2 because their difference would be smaller than their spectral error. Thus, the adoption of the long DE441 ephemeris files was crucial for validating the proposed model based on the orbital near-commensurabilities of Jupiter, Saturn, Uranus, and Neptune.

4. Conclusions

Herein we have studied and modeled the SIM from its frequency domain perspective using the latest JPL ephemeris files that span from from 12999 BC to 16998 AD The 30,000 yr long records allowed us to evaluate high resolution periodograms of the SIM orbits and determine their fine spectral structure. The results demonstrate that the spectral structure of the SIM can be effectively described by the "extended orbital invariant inequality" model described in Equation (7). We provide a brief overview of the primary mathematical properties of the proposed orbital near-commensurability model by demonstrating that it can be conveniently represented and managed through the adoption of a vectorial formulation, which allows for the rapid calculation of each SIM periodicity. This formulation employs the synodic periods of each planet pair as constructors, in addition to the orbital period of a single planet (e.g., Jupiter alone). Moreover, Equation (9) confirms that the SIM frequency clusters are centered around periods given by the harmonic model $P_n \approx 179/(n-1)$ yr (where $n \geqslant 2$ is the cluster order) up to at least the 20th harmonic, as documented in Figure 5 and Table 3. It is worthy of attention to note the two major longer periodicities comprising the Eddy millennial cluster (772.7 and 1159 yr) and the longer Bray-Hallstatt periodicity (2318 yr), which are both clearly detected in solar proxy records (McCracken et al. 2013, 2014), and other important shorter periodicities (Scafetta 2020).

Data Availability

The supplementary file contains the cycle-path records plotted in Figure 2 and the periods of the orbital inequalities depicted in Figures 3 and 4 up to cluster #21.

ORCID iDs

Nicola Scafetta https://orcid.org/0000-0003-0967-1911
Franco Milani https://orcid.org/0000-0001-7721-7214

References

Abreu, J. A., Beer, J., Ferriz-Mas, A., McCracken, K. G., & Steinhilber, F. 2012, A&A, 548, A88
Butkevich, A. G., & Lindegren, L. 2014, A&A, 570, A62
Charbonneau, P. 2022, FrASS, 9, 853676
Charlot, P., Jacobs, C. S., Gordon, D., et al. 2020, A&A, 644, A159
Charvátová, I. 1988, AdSpR, 8, 147
Charvátová, I. 1995, Climatic Change, 29, 333
Charvátová, I. 2000, AnGp, 18, 399
Charvátová, I., & Střeštík, J. 2007, AdSpR, 40, 1026
Cionco, R. G., & Pavlov, D. A. 2018, A&A, 615, A153
Darby, D., Ortiz, J., Grosch, C., & Lund, S. P. 2012, NatGe, 5, 897
De Vries, H. 1958, KNAB, 61, 94
Goldreich, P., & Sciama, D. W. 1965, MNRAS, 130, 159
Fairbridge, R. W., & Shirley, J. H. 1987, SoPh, 110, 191
Gleissberg, W. 1939, Obs, 62, 158
Grootes, P. M., & Stuiver, M. 1997, JGR, 102, 26455
Gray, L. J., Beer, J., Geller, M., et al. 2010, RvGeo, 48, RG4001
Hale, G. E., Ellerman, F., Nicholson, S. B., & Joy, A. H. 1919, ApJ, 49, 153

Jakubcová, I., & Pick, M. 1986, StGG, 30, 224
Jose, P. D. 1965, AJ, 70, 193
Klevs, M., Stefani, F., & Jouve, L. 2023, SoPh, 298, 90
Landscheidt, T. 1999, SoPh, 189, 413
Mayewski, P. A., Meeker, L. D., Twickler, M. S., et al. 1997, JGR, 102, 26345
McCracken, K. G., Beer, J., Steinhilber, F., & Abreu, J. 2013, SoPh, 286, 609
McCracken, K. G., Beer, J., & Steinhilber, F. 2014, SoPh, 289, 3207
Neff, U., Burns, S. J., Mangini, A., et al. 2001, Natur, 411, 290
Ogurtsov, M. G., Nagovitsyn, Y. A., Kocharov, G. E., & Jungner, H. 2002, SoPh, 211, 371
Palus, M., Kurths, J., Schwarz, U., et al. 2007, PhLA, 365, 412
Perryman, M. A. C., & Schulze-Hartung, T. 2011, A&A, 525, A65
Schwabe, M. 1844, AN, 21, 234
Scafetta, N. 2012a, JASTP, 80, 296
Scafetta, N. 2012b, JASTP, 81, 27
Scafetta, N. 2014, PRP, 2, 1
Scafetta, N. 2020, SoPh, 295, 33
Scaffetta, N. 2023, SoPh, 298, 24
Scafetta, N., & Bianchini, A. 2022, FrASS, 9, 937930
Scafetta, N., Milani, F., Bianchini, A., & Ortolani, S. 2016, ESRv, 162, 24
Shirley, J. H., Sperber, K. R., & Fairbridge, R. W. 1990, SoPh, 127, 379
Stefani, F., Giesecke, A., & Weier, T. 2019, SoPh, 294, 60
Stefani, F., Horstmann, G. M., Klevs, M., Mamatsashvili, G., & Weier, T. 2024, SoPh, 299, 51
Sonett, C. P., & Finney, S. A. 1990, PTRSA, 330, 413
Suess, H. E. 1980, Radcb, 22, 200
Willson, C. 1985, AHES, 33, 15
Wilson, I. R. G., Carter, B. D., & Waite, I. A. 2008, PASA, 25, 85
Wolf, R. 1859, MNRAS, 19, 85
Zaqarashvili, T. V. 1997, ApJ, 487, 930